Effect of Particle Size Distribution on Isothermal Oxidation Characteristics of Plasma Sprayed CoNi- and CoCrAlY Coatings

Dowon Seo, Kazuhiro Ogawa, Tetsuo Shoji, and Shozo Murata

(Submitted March 11, 2007; in revised form August 9, 2007)

The effect of particle size distribution on the degradation behavior of plasma sprayed CoNi- and CoCrAlY coatings during isothermal oxidation was investigated, in terms of the oxygen content, porosity, surface roughness, and oxide scale formation. The results show that the degradation of both coatings was considerably influenced by the starting particle size distribution. It also shows that in the as-sprayed vacuum plasma spray (VPS) coatings the oxygen content on the coating surface increased significantly with decreased average particle size. But after thermal exposure, the difference of the oxygen contents between the coatings with different particle size was decreased. The powder with various particle size resulted in low porosity inside the coatings during the deposition process. The surface roughness of the coatings increased with increased particle size. The small particles produced a relatively smooth surface, and the oxide growth in the coating deposited by small particle was slower than that in the large particle coating.

1. Introduction

MCrAlY (where M is the alloy base metal; typically nickel (Ni), cobalt (Co), or combination of these two) metallic overlay coatings protect the hot-section components, such as blades and vanes, in gas turbine engines against high temperature oxidation and hot corrosion attack together with thermal barrier coatings (TBCs). These coatings provide a way of extending the limits of use of materials at the upper end of their performance capabilities, by allowing the mechanical properties of the

Dowon Seo, Kazuhiro Ogawa, and **Tetsuo Shoji**, Fracture & Reliability Research Institute, Tohoku University, Aoba 6-6-01, Aramaki, Aoba-ku, Sendai 980-8579, Japan; and **Shozo Murata**, Murata Boring Technology Research Co., Ltd, Kitamaruko 1-30-45, Suruga-ku, Shizuoka 421-0106, Japan. Contact e-mail: seodw@rift.mech.tohoku.ac.jp.

substrate materials to be maintained while protecting them against oxidation or corrosion (Ref 1, 2). Failure of a MCrAlY coating usually occurs by delamination of the thermally grown oxide (TGO) scale that forms at the coating surface, during high-temperature exposure. The cracks leading to the delamination nucleate and propagate at the TGO-overlay coating (Ref 3). Thus, a slow-growing dense oxide scale is desirable to ensure a longer lifetime of the MCrAlY coating. It is preferred that this oxide scale be a continuous, dense α-alumina (α-Al$_2$O$_3$) layer (Ref 4), since it protects the metallic overlay coating from further oxidation, due to the low diffusivity of oxygen and metallic elements through the α-alumina layer (Ref 5). However, many factors, such as starting powder (Ref 6-8), alloy chemistry (Ref 9-12), microstructure of the coating (Ref 13, 14), surface condition of the deposited coating (Ref 15-17), deposition method and its process parameters (Ref 18-20) can affect the composition and the structure of the TGO scale that in turn, can greatly affect the performance of the MCrAlY coatings.

Particularly, the particle size of starting powders, along with the chemical composition, plays an important role on the coating properties. Previous work that aimed at identifying the mechanism responsible for splat deposition has focused largely on particle size effect (Ref 6-8, 21-24). The oxygen content in the as-sprayed coating depends on the spraying technique, spraying parameters, and starting material compositions (Ref 18, 23, 25, 26). Espie et al. (Ref 21-23) reported that the oxygen content in air plasma sprayed (APS) low carbon steel particles increased with spray distance. Fukushima and Kuroda (Ref 26) presented similar result for high velocity
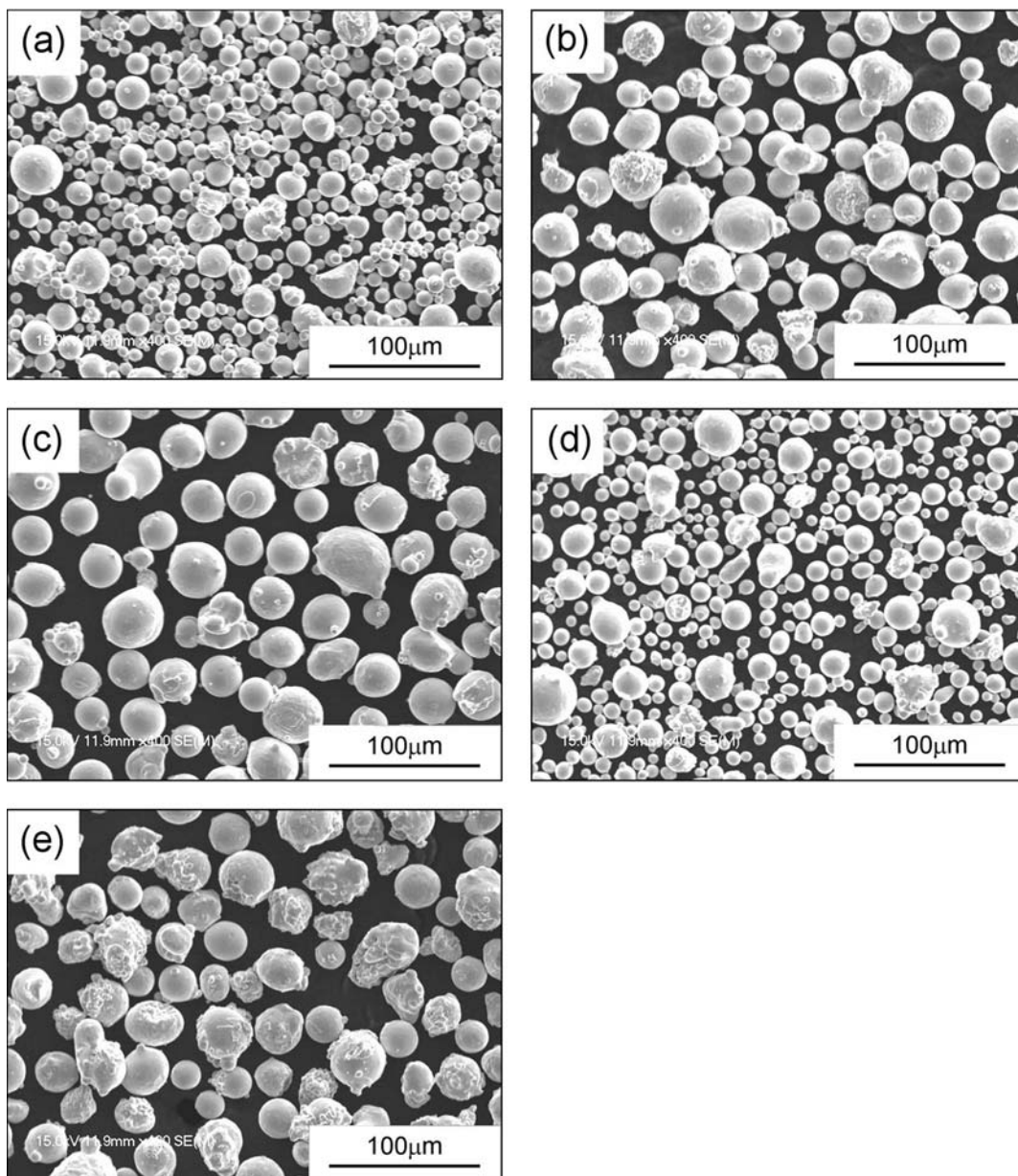
Fig. 1 Morphology of the spray powders: (a) CONI-S; (b) CONI-M; (c) CONI-L; (d) CO-S; (e) CO-L

Table 1 Nominal compositions and coating thickness of the as-sprayed coatings

| Type	Designation	Chemical composition (a), wt.%					Average coating thickness, μm	Manufacturer
		Co	Ni	Cr	Al	Y		
CoNiCrAlY	CONI-S	38.5	32	21	8	0.5	269	Sulzer Metco
	CONI-M	38.5	32	21	8	0.5	247	Praxair Tech
	CONI-L	37.5	33	21	8	0.4	308	Carpenter Tech
CoCrAlY	CO-S	63.3	…	23	13	0.7	266	Praxair Tech
	CO-L	63.4	…	23	13	0.6	316	Carpenter Tech

(a) Specified by supplier

oxygen-fuel (HVOF) sprayed Ni-20Cr coating, but they also reported that the oxygen content in the HVOF-sprayed coating was decreased with stand-off. From this result (Ref 26), it can be found that the oxygen content reached up to 10 wt.% in HVOF-sprayed coatings, while the oxygen contents in most coatings deposited under

Table 2 Particle size ranges and descriptive statistics of powders, μm

Designation	Norminal range (a)	Analyzed range	Range	Mean	Median	Std. deviation	Sample variance	Std. error
CONI-S	−35 + 5	−34.5 + 2.5	32.06	9.40	8.375	4.22	17.80	0.16
CONI-M	−45 + 10	−43.5 + 3.6	39.86	20.51	20.35	8.36	69.95	0.75
CONI-L	−45 + 22	−40.3 + 6.2	34.1	24.84	26.34	7.59	57.55	0.84
CO-S	−44 + 5	−38.4 + 2.0	36.39	10.08	8.58	4.79	22.99	0.22
CO-L	−45 + 15	−44.7 + 12.6	32.06	25.71	25.04	6.51	42.33	0.72

(a) Specified by supplier
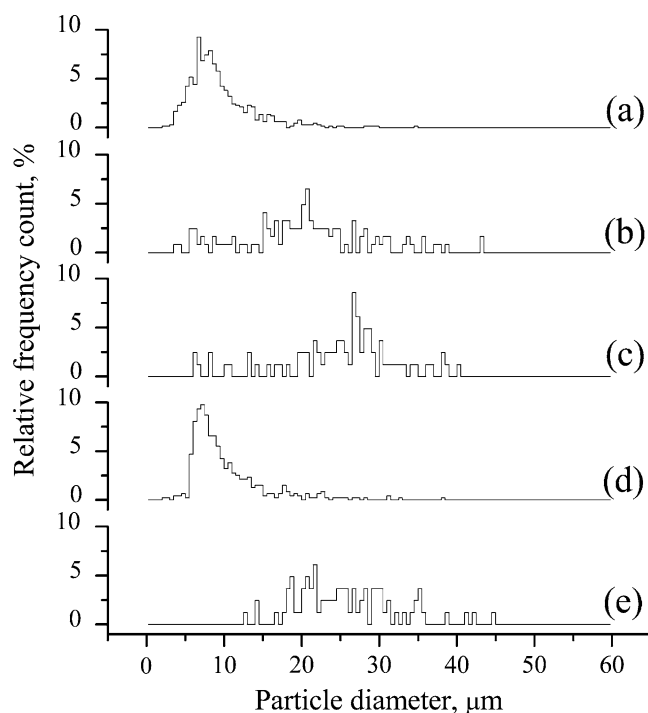
Fig. 2 Particle size distributions of the spray powders: (a) CONI-S; (b) CONI-M; (c) CONI-L; (d) CO-S; (e) CO-L

different conditions were fewer than 0.5 wt.%. However, some other researchers reported an oxygen intake of up to 3-6 wt.% in the coating deposited by HVOF process (Ref 27, 28). These studies also suggested that the difference in grain size of the spray powder may be responsible for the notable difference in coating oxygen content and subsequent oxidation behavior. It can be expected that the properties of the coatings produced by vacuum plasma spray (VPS) process are also affected by particle size, even though a vacuum process can suppress the oxidation of metallic coatings more efficiently during spraying, compared to air plasma spray (APS) and HVOF processes. These previous works focused on in-flight oxidation of particles (Ref 6, 22-23), splat formation (Ref 7, 24), and as-sprayed microstructure (Ref 8). However, it is also important to understand the particle size effect on the oxidation behavior of the coatings and their properties at high temperature. This information can be helpful for end-users to choose the suitable powders. Therefore, in the present study, the influence of particle size on the oxidation behavior of MCrAlY coatings was investigated. The influence of particle size on the oxygen content, porosity, surface roughness, and TGO growth are also examined.

2. Materials and Experimental Procedures

Five commercially available CoNi- and CoCrAlY powders of different size ranges, from several micrometers to over 45 μm, were used as starting materials. Table 1 shows the nominal compositions of the starting powders and the coating thickness of the five as-sprayed coatings, referred as CONI-S, CONI-M, CONI-L, CO-S, and CO-L. All powders were manufactured through gas atomization process. In order to obtain a reliable relationship between particle size and oxygen content, the particle size of the powders was measured statistically from scanning electron microscopy (SEM, Hitachi S-4700, Japan) images. The Inconel 718 alloy (MA718, Mitsubishi Materials Co., Japan) was used as substrate to deposit the coating, which is widely used for gas turbine components. The chemical composition of the substrate material was 19Cr-19Fe-5.1Nb-3Mo-0.9Ti-0.5Al-balance Ni. The VPS processes (A-2000V, Plasma Technik, Germany) were carried out under the following conditions: preheating temperature 843 K during transferred arc treatment, voltage 56-57 V, current 580-590 A, spraying distance 310 mm, argon gas atmosphere 8 kPa.

To characterize the oxidation behavior, static oxidation experiment was carried out in air under isothermal conditions at 1273 K up to 1000 h. Each exposure condition consisted of about 32 K/min heating rate in a kanthal muffle furnace, and about 3 K/min cool-down to ambient temperature. After exposure, the oxidized samples were analyzed by energy dispersive X-ray analysis (EDX, Oxford 6841, USA). Electron spectroscopy for chemical analysis (ESCA, PHI Quantum 2000, USA) was also used to obtain surface profile information in the first few layers, especially oxygen concentration profile. The porosity measurements were made with image analyzer software (ImageJ, NIMH, USA), which is based on ASTM B276. The image was obtained through the SEM. After preliminary characterization, the samples were cross-sectioned, mounted in a conductive, phenolic resin with carbon filler and subjected to mirror polishing to identify the cross-sectional details. The TGO and coating thickness were measured by taking a back scattered
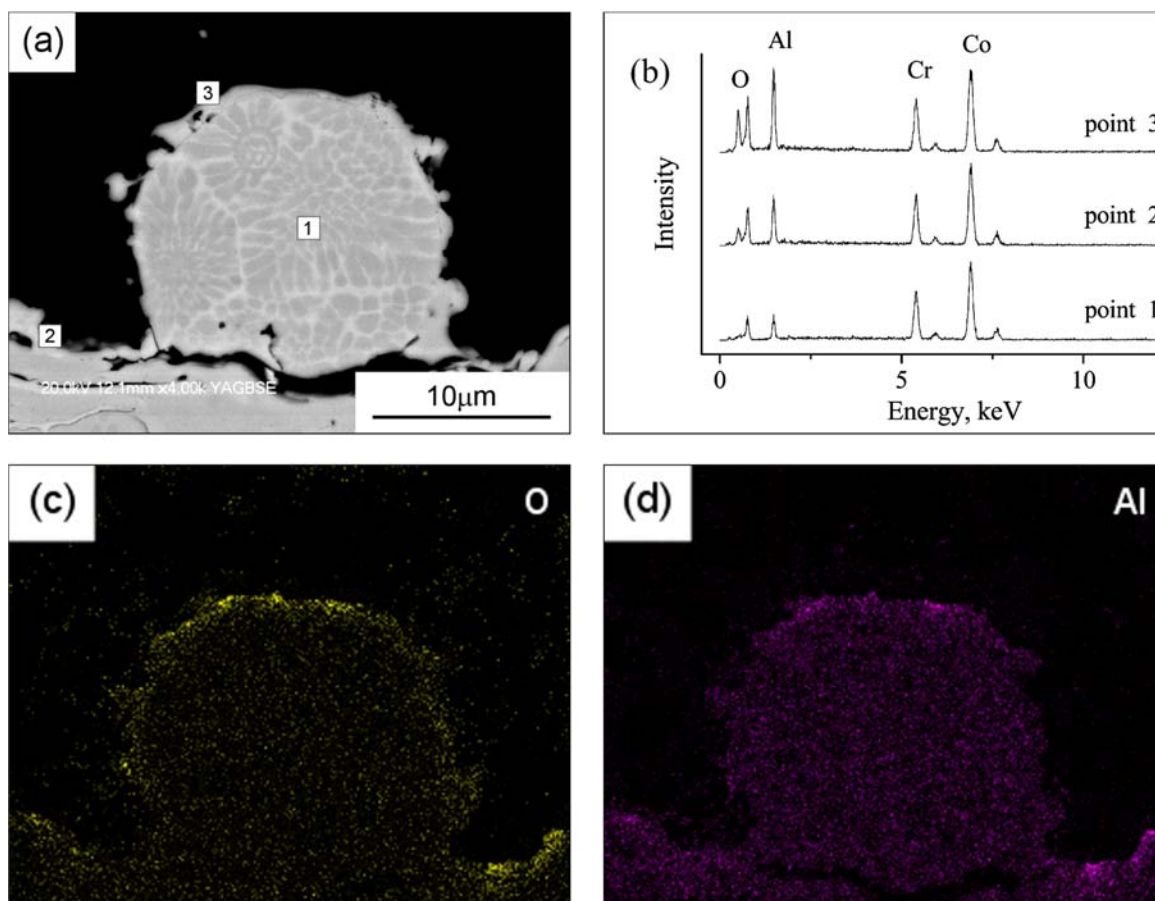
Fig. 3 Cross-sectional microstructure of a deposited particle using (a) CONI-M powder and (b) EDX spectrum analysis results at the center (point 1), near periphery (point 2) of un-melted particle, and fully melted splat (point 3); and corresponding elemental maps of (c) O and (d) Al
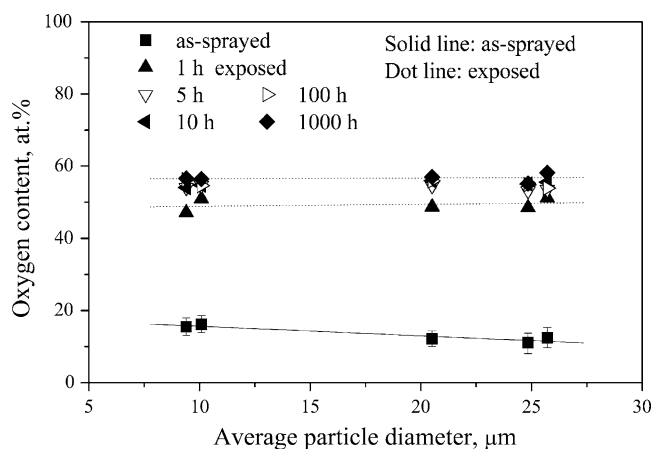

Fig. 4 Effect of particle size on the oxygen contents on the surfaces of CONI- and CO-series coatings

electron image (BSEI) with the SEM, equipped with a Robinson back scattered detector (RBSD). The average thickness was determined by measuring more than 15 images for each sample. The surface roughness of the coatings was measured by the contactless measuring system (Mitaka NH-3T, Japan).

3. Results and Discussion

3.1 In-flight Oxidation

Figure 1 shows the typical morphology of spray powders in different size distribution. It can be found that all powders had a spherical shape. The measured particle size is shown in Table 2 and Fig. 2. From these results, it is clear that the measured mean particle size was smaller than the mean value of the opening sizes of the sieves specified by suppliers. The CONI-S and CO-S powders had the smallest particle size and narrowest particle size distribution.

Figure 3 shows a cross-section of a collected particle of approximately 28 μm in diameter and the EDX results obtained at three typical locations. It was found that there was a thin-splat-shell covering over the particle, which consisted oxides that formed during spraying process (point 3, Fig. 3a). No evidence of oxygen was
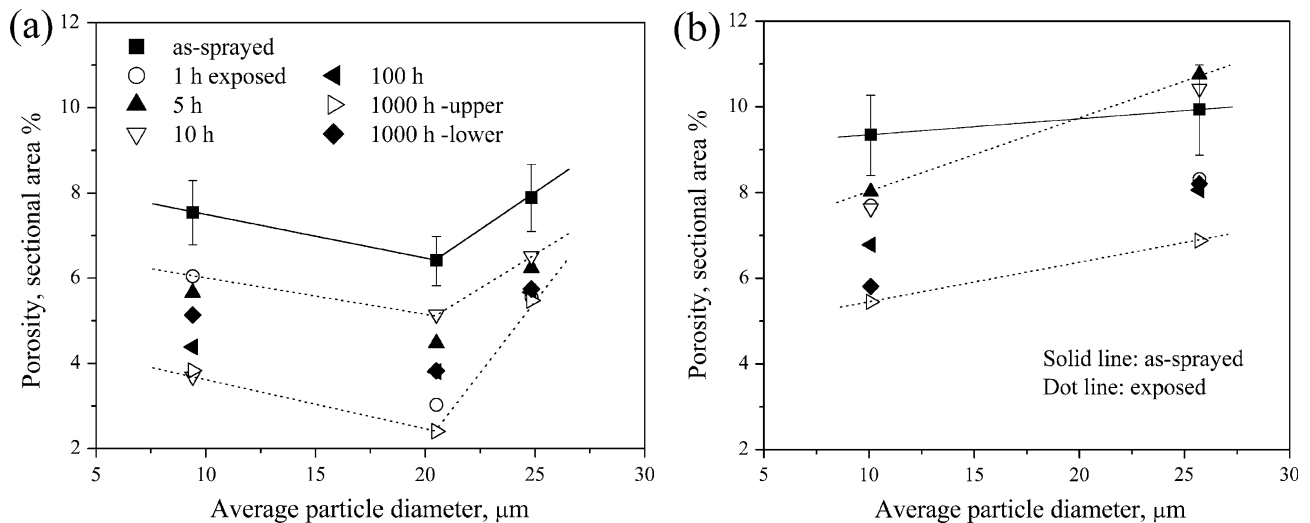
Fig. 5 Effect of particle size on the porosity of (a) CONI- and (b) CO-series coatings with thermal exposure

found inside the particle as shown in the point 1 of Fig. 3(b). This result suggested that there is an interface between the oxide surface covering and the non-oxidized inner fraction of the particle, as shown in Fig. 3(c) and (d). Therefore, in spite of VPS, the oxidation of an in-flight particle proceeds from particle surface toward the inside. As the result of referred research, Li et al. (Ref 6) showed a HVOF sprayed particle, and its EDX analysis showed that the thin-film-shaped covering was an oxide film formed during in-flight. During the in-flight stage, the oxygen content in the powders increases with decreased particle size. To examine the oxidation behavior of spray powder during in-flight, the powders passing through flame can be collected by spraying into water (Ref 6). From its results, the oxygen content in the as-sprayed coating is equal to that in the collected powders when the mean particle size is fewer than 45 μm (Ref 6). So, the oxygen content only on the as-sprayed coating was measured, because the mean diameters of all samples are fewer than 45 μm. When the mean particle size of powders was reduced to approximately 30 μm, a rapid increase in oxygen content in the in-flight powders would occur (Ref 6). It is clear that the particle size has a significant effect on the oxidization of the in-flight particle and consequently the oxygen content in spraying powders.

Generally, the oxidation of an alloy particle in a flame occurs on the particle surface. The oxygen content in the particle will increase with time because of the diffusion of oxygen from the surface toward the inside of the particle. Based on the relation between the oxygen content in an in-flight particle and the distance for plasma spraying (Ref 23), it can be considered that the oxygen content in the particle would follow the parabolic law, although the effect of internal flow in a fully melted particle may occur and intensify the oxidation by exposing the fresh metal surface to the flame as pointed out (Ref 23, 29). Therefore, at the initial stage, the oxygen content in the particle will increase rapidly. As the oxidation further proceeds, the

increase in oxygen content will become less intensive. Moreover, after the particle flies off the high-temperature zone of the flame, oxidation becomes slower.

Figure 4 shows the oxygen contents on the coating surfaces versus the average particle size of the powder. The oxides on the surfaces of the as-sprayed coatings are resulted from the oxidation of powders. It can be seen that the oxygen contents on the CONI-S and CO-S coating surfaces were higher than those on the other coatings. It can be clearly observed that a significant increase in the oxygen content on the coating surface occurred with decreased average particle size. When the average particle size was approximately 10 μm, the oxygen content (15.5 at.% in case of CONI-S) was 27.3% higher than the coating deposited by the powders larger than 20 μm (12.18 at.% in case of CONI-M), suggesting that the particle size of powder has a substantial effect on the oxygen content on the deposited coating surface. This explains why the coatings deposited by the same type of material may significantly differ in the oxygen contents. Therefore, when the spray materials with grain size of fewer than 40 μm are used and the oxidation is involved, the particle size and the distribution of the size as well should be taken into account essentially.

After thermal exposure, the difference of the oxygen contents between the smaller and larger particle coatings was decreased with increased exposure time. Generally, the oxide scale growth in isothermal condition initiates on the free surface of coating. Therefore, at the initial stage (1 h), the oxygen content increased rapidly. As the oxidation proceeded, the increase in oxygen content became less intensive. Because the EDX beam focused on the oxide scale of the thermal-exposed surface. The oxide products in MCrAlY coatings are $(Cr,Al)_2O_3$, $(Co,Ni)(Cr,Al)_2O_4$ and $(Cr,Ni)O$, they all have an oxygen content from 50 to 60 at.%, which agrees with the result of this study (Fig. 4). Therefore, it can be expected that the oxygen content in the oxide scale would not change much
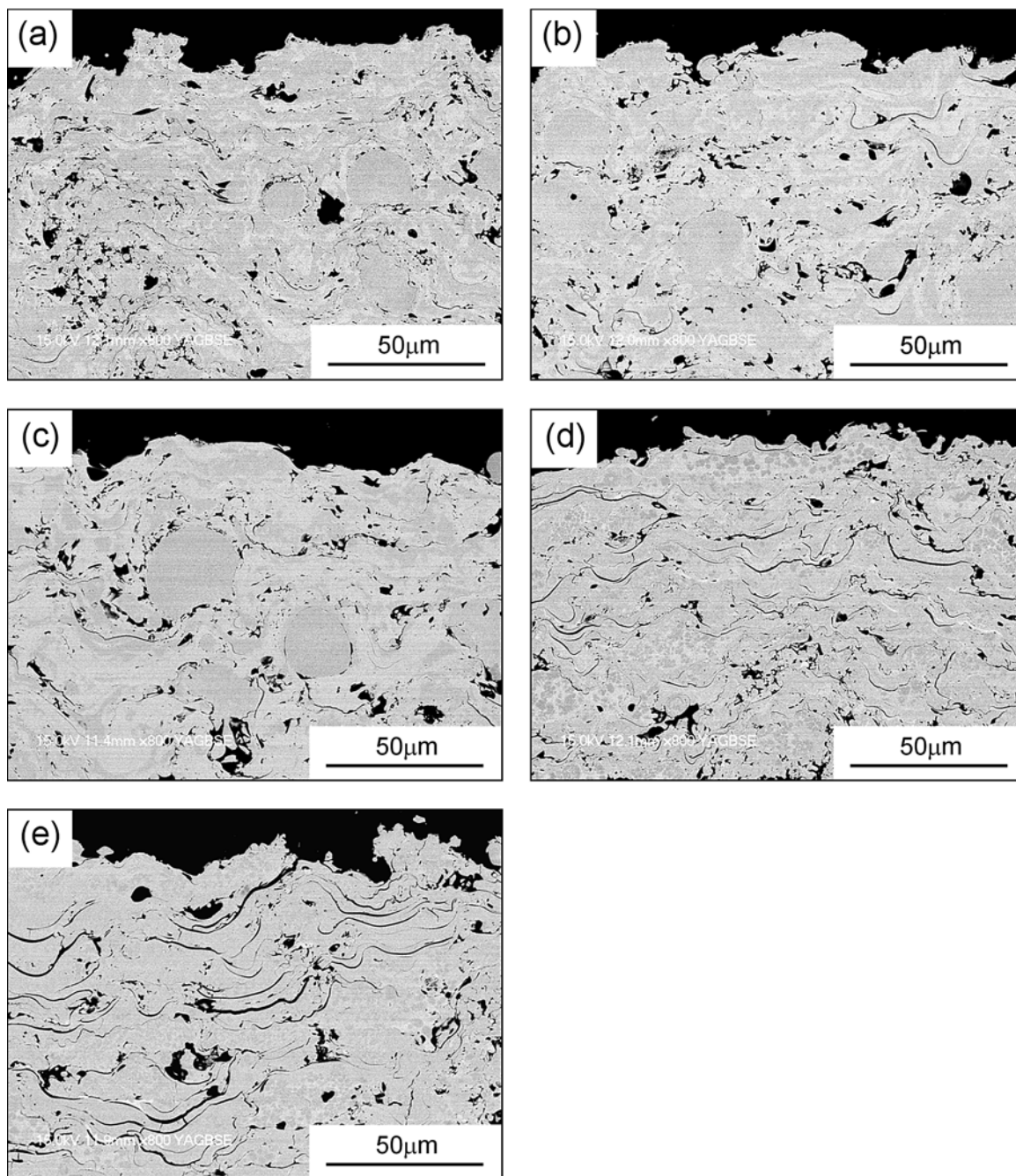
Fig. 6 Microstructures of as-sprayed coatings: (a) CONI-S; (b) CONI-M; (c) CONI-L; (d) CO-S; (e) CO-L

after extended thermal exposure. In the meantime, the influence of particle size on the oxygen content on the thermal-exposed coating surface also became less significant as shown in Fig. 4.

3.2 Cross-Sectional Porosity

Figure 5 shows the distribution of the cross-sectional porosity in the coating within 50-150 μm from the coating surface as a function of particle size. The amount of

porosity increased normally with increased particle size. This, of course, could be due to the reduced melting efficiency of the coarser particles in the plasma plume. The coating produced by finer powder showed well-adhered splats, while the inter-splat pores were more prominent in the CO-series coatings, as shown in Fig. 6(d) and (e). The unmelted and poorly adhered particles could be seen in the coarse powder coatings. Earlier studies (Ref 20) showed that the morphology of the splats changed from a contiguous disk-like shape to a fragmented shape with
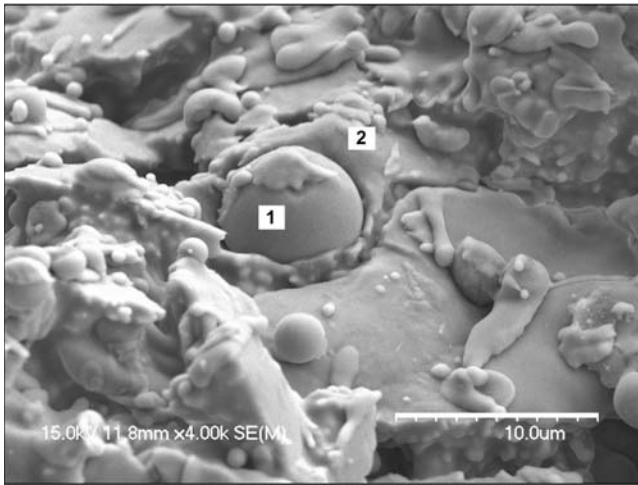
Fig. 7 Compressing phenomenon of the as-sprayed CONI-series coatings: (1) an unmelted particle; (2) the pressed splat by the particle

increased particle size. These fragmented splats led to poor splat–splat adherence and consequently the formation of pores. In addition to the particle size, the distribution of particle size might also play an important role in coating porosity. In some cases, the unmelted particles, i.e., the relatively large particles in distribution, press the splats and make the poorly bonded splat–splat contact closed, as shown in Fig. 7. The CONI-M coating had the lowest porosity (Fig. 5a), which could be due to the good accommodation among the particles of different size, since this powder had the widest particle size distribution, as shown in Table 2.

As shown in Fig. 5 and 8, with increased exposure time, the amount of porosity decreased gradually in all coatings. As presented in the authors' previous work (Ref 30), the porosity decreased through several time stage. The fast change of porosity after short sintering times was also observed. It could be expected that short exposure to high temperatures is sufficient to heal cracks and bind splats together, leading to decreased porosity inside the MCrAlY coatings (Ref 31).

Figure 9 shows sketches of the mixed powders of different sizes, where L, M, and S represent the large (−45.0 + 30.6 μm), middle (−30.6 + 16.3 μm), and small (−16.3 + 2.0 μm) particles, respectively. It can be seen that the tri-modal arrangement results in the lowest apparent porosity (14.42 area%; Fig. 9b), while the bi-modal, i.e., mono-sized middle particles with one small particle yields the highest apparent porosity (30.44 area%; Fig. 9c). From the powder metallurgy viewpoint, the plain tri-modal is an ideal situation for high compaction shown in Fig. 9(b) where the small particles just touches the large neighboring particles. The apparent density of the coating can be influenced by many factors, such as particle size, shape, size distribution, inter-particle friction, surface chemistry, agglomeration and packing type, etc. (Ref 32). In general, it can be expected that the packing density decreases with decreased particle size, due to the higher inter-particle

friction, and spherical shaped particles lead to a higher density. Mixing of powders with different size may result in higher apparent density, by filling the voids between the large particles with finer ones. Moreover, surface roughness and irregular shape of the powders may reduce the packing density.

3.3 Surface Roughness and Oxide Formation

Figure 10 shows the surface morphology of the as-sprayed CoNi- and CoCrAlY coatings. Some unmelted or partially melted particles can be seen on the coated surfaces of CONI-series coatings as shown in Fig. 10(a-c). These unmelted particles resulted in rough coating surfaces in contrast to the CO-series coatings with relatively well-melted particles as shown in Fig. 10(d) and (e). The surface roughness of the coating increases with increased powder size (Fig. 11), which is consistent with previous observations (Ref 15-17). CO-series coatings have lower surface roughness compared with CONI-series coatings within similar particle size, because of the relatively well-melted lamellar structure. After the thermal exposure, the surface roughness decreased in both CONI- and CO-series coatings, while the coatings produced by larger particles had higher surface roughness. Over the 1 h exposure, surface roughness was kept in relatively constant zone, and the sharp drop of the surface roughness at the initial exposure time is due to the TGO, i.e., the growth of spinel-type oxide and/or Al_2O_3 on the surface, as presented in the previous work (Ref 30). The open pores of the surface could be filled with these oxides including the partial sintering phenomenon of inter-splat pores (Ref 30). Tang et al. (Ref 2) also showed that the oxide scale grown on the CoNiCrAlY coating consisted primarily of spinel-type oxides after 1 h exposure at 1273 K. After extended thermal exposure, in addition to the spinel-type oxides, α-alumina and Cr_2O_3 were also identified (Ref 2, 30). The crystal size of these TGO scales is relatively smaller than the irregularities of the as-sprayed surfaces, so the thermally exposed surface becomes smooth gradually (Ref 30). For this reason, the effect of particle size on the surface roughness of the exposed coatings remains the same as the as-sprayed coatings.

The TGO thickness and weight gain plots for the CONI- and CO-series coatings in static air at 1273 K are shown in Fig. 12 and 13, respectively. CO-series coatings exhibit a higher value level of the oxide scale thickness and the weight gain than CONI-series coatings. The average values of the TGO thickness were proportional to the particle size after 50 h of thermal exposure, and the average values of weight gain were also proportional to the particle size. However, TGO thickness decreased with increased particle size within the very early transient oxidation stage (up to 10 h of thermal exposure). For example, at 1 h of thermal exposure, the average TGO thicknesses of small particle coatings (1.77 μm for CONI-S; 2.0 μm for CO-S) were thicker, compared with the large particle coatings (1.46 μm for CONI-L; 1.77 μm for CO-L). The small particles produce a relatively smooth surface, and then the coatings have a low surface roughness
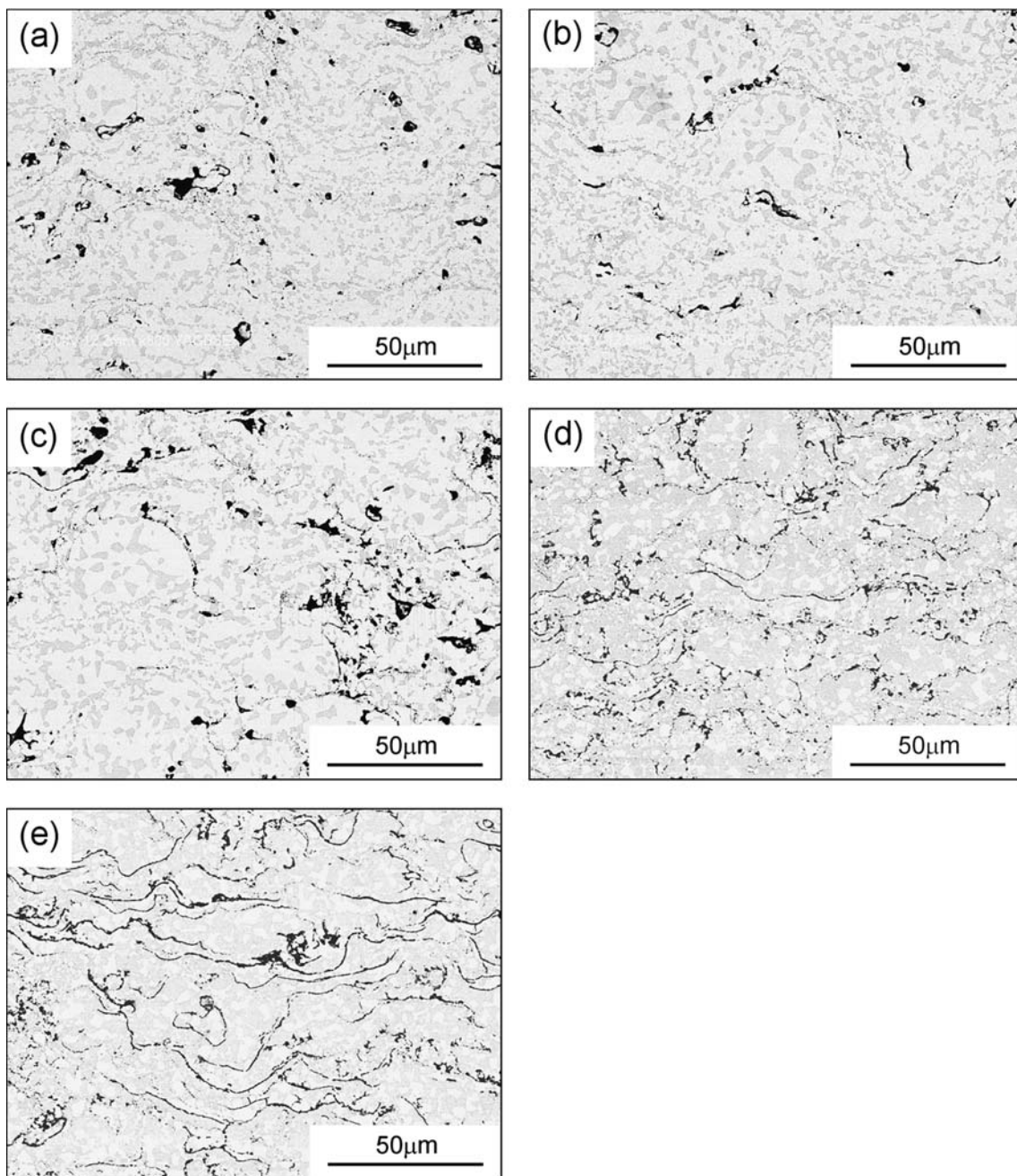
Fig. 8 Inside-pore microstructures of the 100-hour exposed coatings: (a) CONI-S; (b) CONI-M; (c) CONI-L; (d) CO-S; (e) CO-L
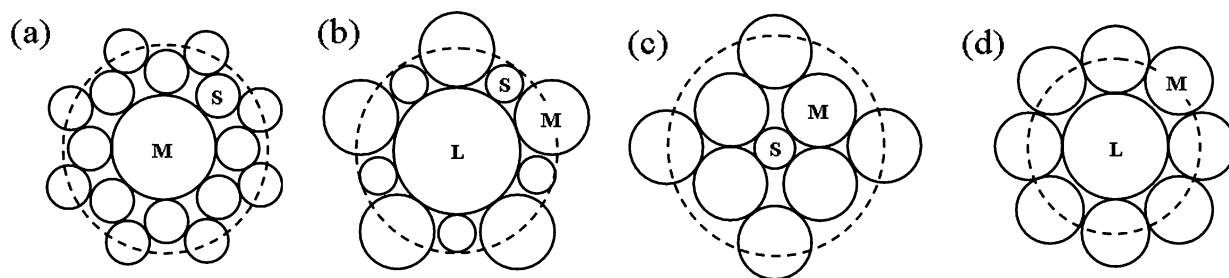

Fig. 9 Plain bi- and tri-model of powder packing for: (a) CONI-S; (b) CONI-M and CONI-L; (c) CO-S; (d) CO-L
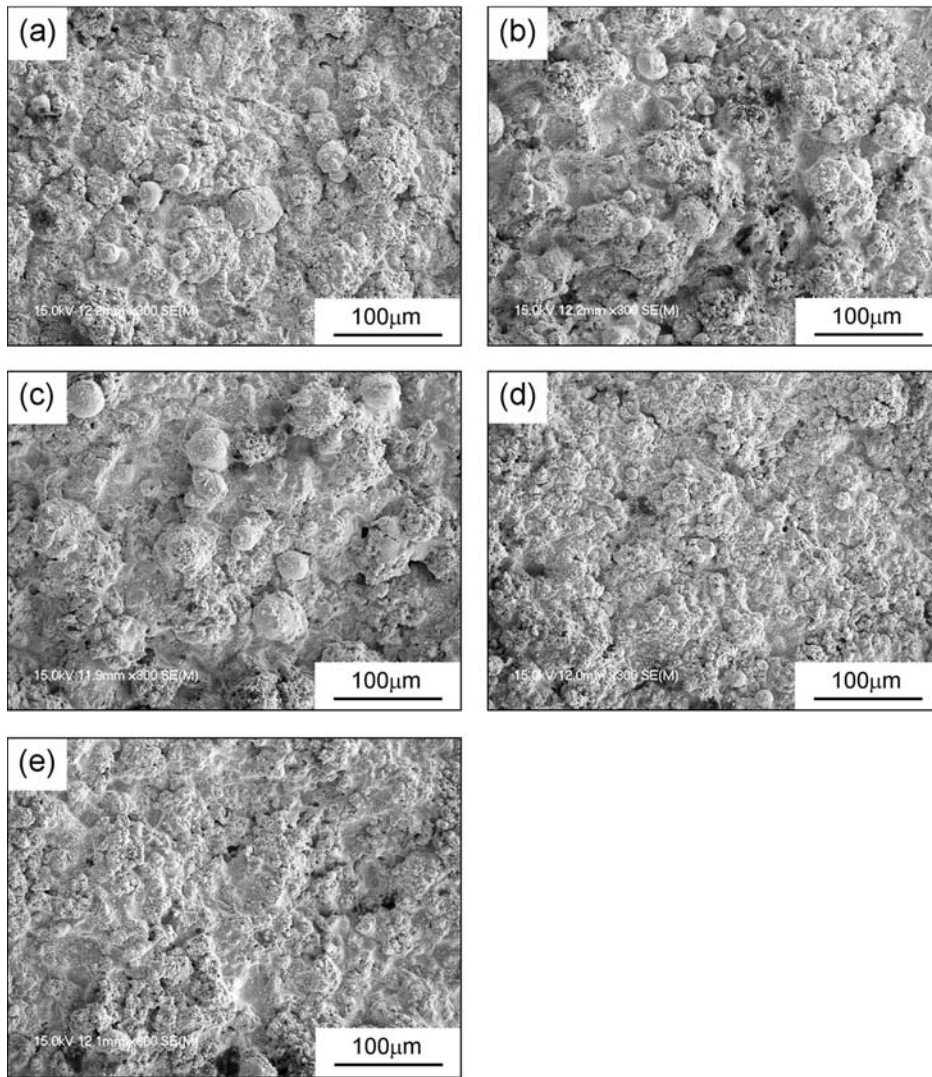
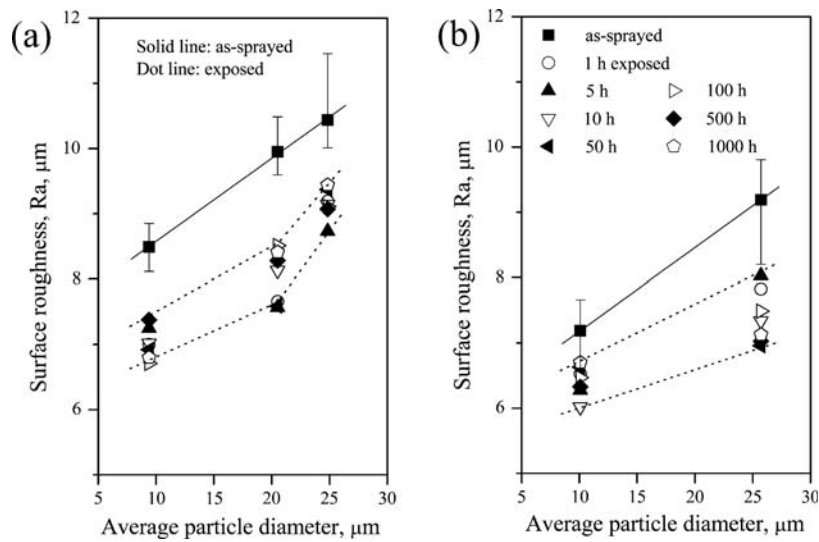**Fig. 10** Surface morphology of the as-sprayed coatings: (a) CONI-S; (b) CONI-M; (c) CONI-L; (d) CO-S; (e) CO-L

Fig. 11 Effect of particle size on the surface roughness of (a) CONI- and (b) CO-series coatings with thermal exposure
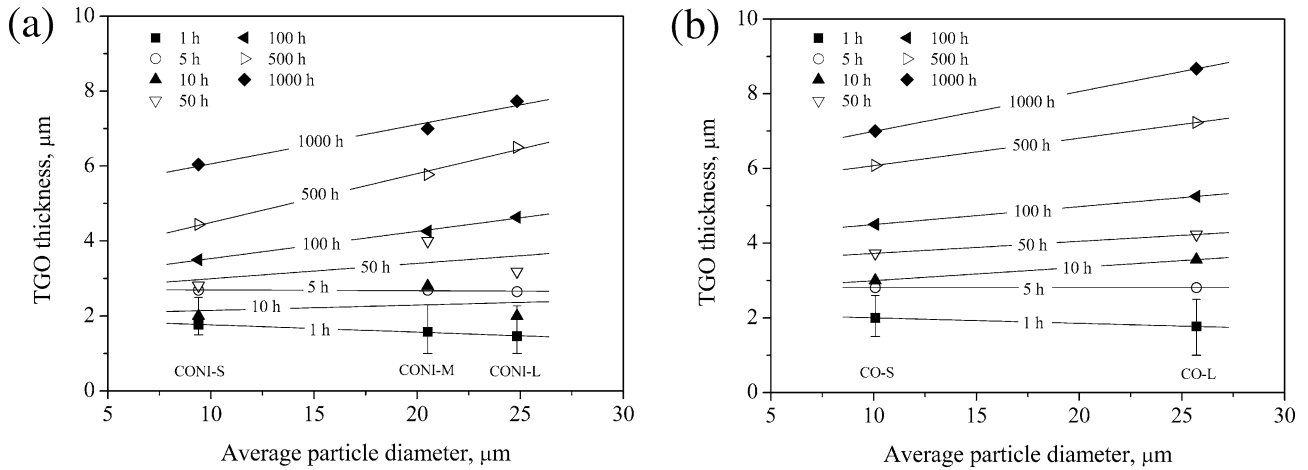
Fig. 12 Effect of particle size on the TGO thickness of thermal exposed (a) CONI- and (b) CO-series coatings
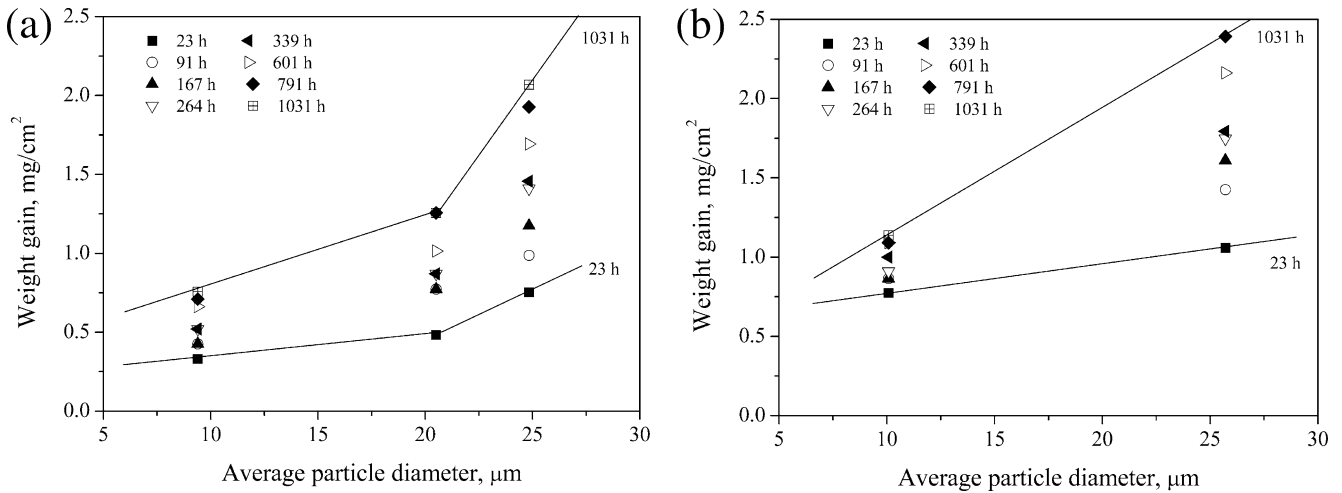

Fig. 13 Effect of particle size on the weight gain of thermal exposed (a) CONI- and (b) CO-series coatings

leading to the rapid attainment of the steady-state oxidation stage (Ref 15, 16, 33). The initially formed continuous alumina film acts as a barrier preventing the coating from further oxidation. One possible mechanism is blocking lattice diffusion through the scale thereby reducing its growth rate (Ref 34). The distribution range of TGO thickness and weight gain extended with increased particle size as shown in Fig. 12 and 13.

The oxidation can be divided into two stages (Ref 35): one is the transient oxidation stage, which shows a relatively rapid oxidation rate and the other is the steady-state oxidation stage, which shows a relatively slow oxidation rate. The transition time from the initial transient oxidation to the steady-state oxidation can be defined as the time of intersection of the extrapolation lines of the initial rapid oxidation and that of the steady-state oxidation. The transition times for all the coatings were within 23-91 h, as can be seen in Fig. 14. CONI-L and CO-L coatings showed a faster oxidation rate than other coatings as
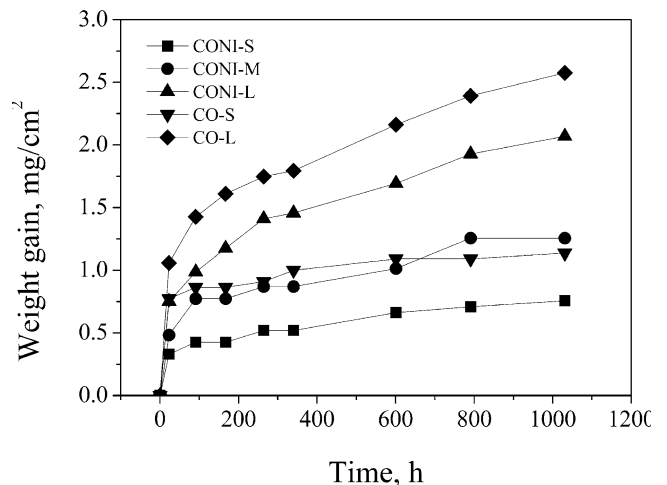

Fig. 14 Oxidation kinetics of thermal exposed CONI- and CO-series coatings
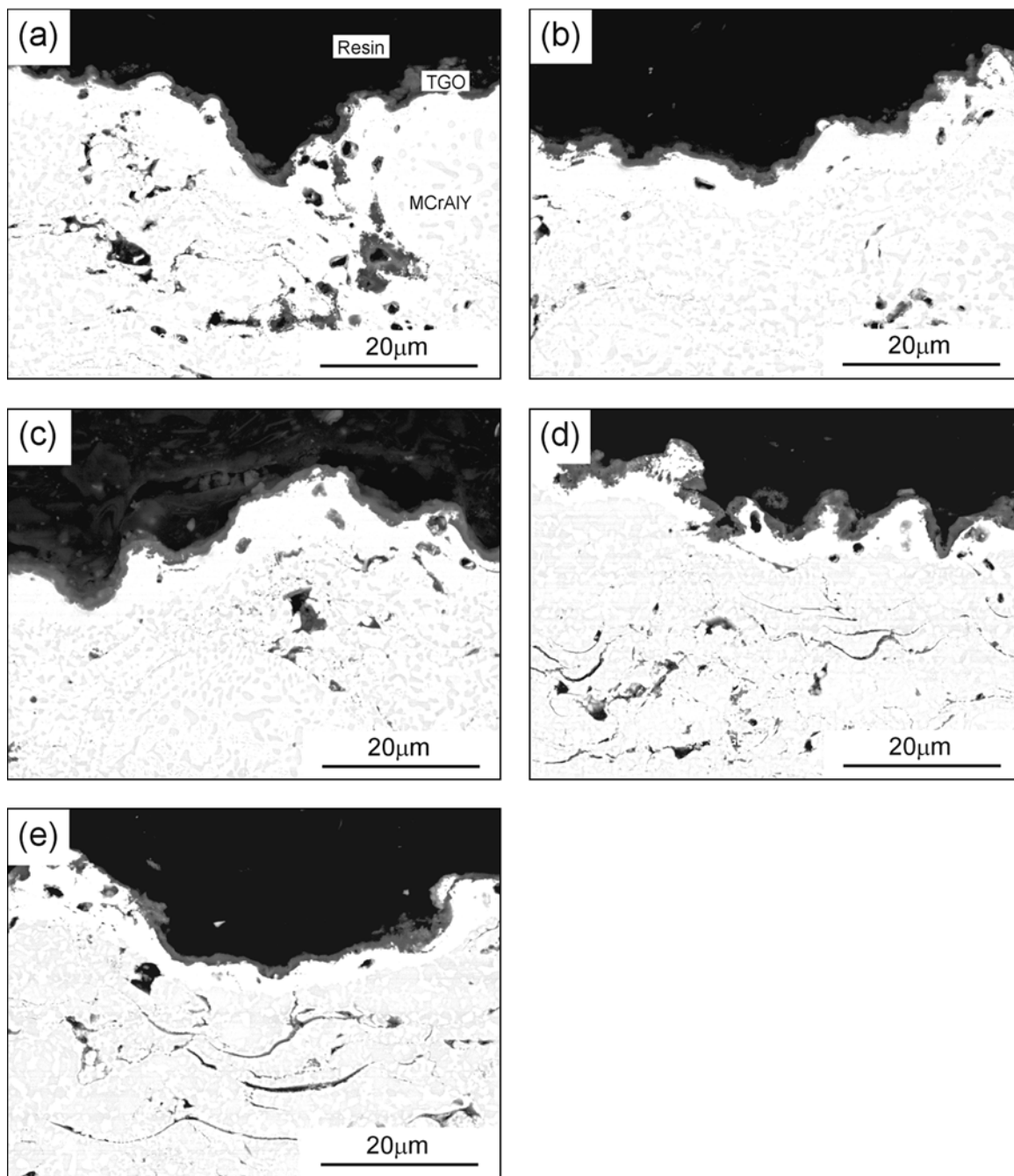
Fig. 15 TGO formation on the coating surface after 1 h thermal exposure: (a) CONI-S; (b) CONI-M; (c) CONI-L; (d) CO-S; (e) CO-L

shown in Fig. 14, which might be due to the bigger particle size and higher surface roughness shown in Fig. 11.

Figure 15 shows the cross-sectional BSE micrographs for CONI- and CO-series coatings showing the TGO formation after 1-hour thermal exposure. The micrographs of the TGO scales show a coherent alumina scale (black regions marked as TGO) on all coatings. After only 1 h exposure, TGO was rapidly formed relatively to the steady-state oxidation stage. The scale thickness ranged from 1.46 μm (CONI-L; Fig. 15c) to 2.0 μm (CO-S;

Fig. 15d). TGO scale grew slowly in the steady-state oxidation stage (over 23-91 h) as shown in Fig. 14. After 100 h exposure, TGO thickness ranged from 3.5 μm (CONI-S; Fig. 16a) to 5.25 μm (CO-L; Fig. 16e). Further oxidation caused the development of less protective spinel-type mixed oxides near the coating surface as shown in Fig. 16 (light gray regions, indicated by arrow marks). This mixed oxide consists of Co-Ni-Cr-Al-O oxide system, i.e., NiO, CoO, Cr_2O_3, (Ni, Co) (Cr, Al)$_2O_4$, and so on (Ref 12). All of the coatings appeared to be adhered to the
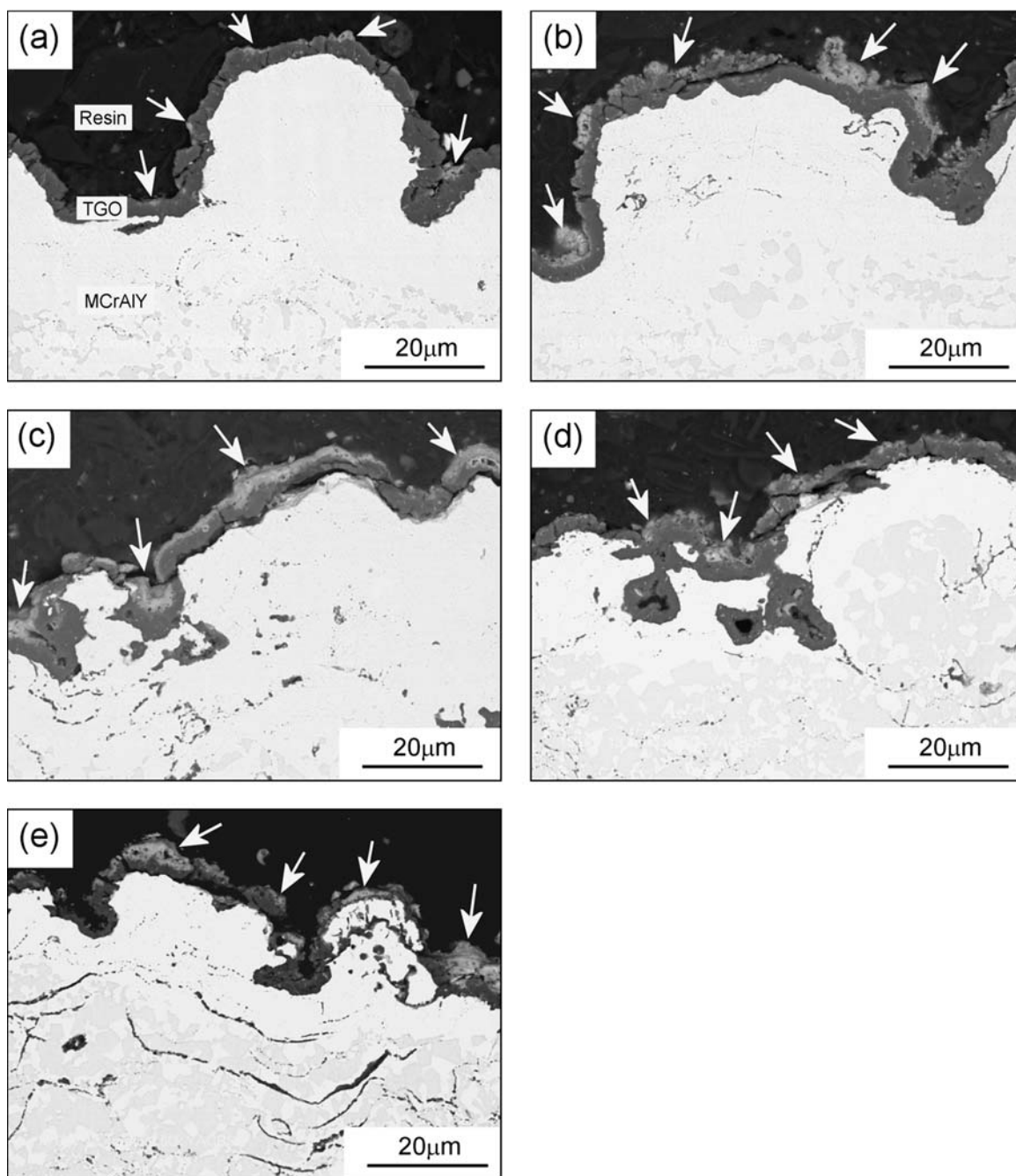
Fig. 16 TGO formation on the coating surface after 100 h thermal exposure: (a) CONI-S; (b) CONI-M; (c) CONI-L; (d) CO-S; (e) CO-L

substrate, although small cracks were observed near the mixed spinel oxides during the isothermal oxidation.

4. Conclusions

The particle size has a significant effect on the oxygen content on the as-sprayed coating surface. But after thermal exposure, the difference of the oxygen contents between the smaller and larger particle coatings was decreased with increased exposure time. The distribution of particle size plays the important role of porosity. The porosity decreased gradually in all coatings with increased exposure time. Surface roughness of the thermal exposed coatings increased with increased particle size. The small particles produce a relatively smooth surface, and then the coatings have a low surface roughness leading to the slow

TGO growth upon thermal exposure. TGO thickness was proportional to the particle size and increased exposure time, and the weight gain was also proportional to the particle size.

References

1. P.S. Sidky and M.G. Hocking, Review of Inorganic Coatings and Coating Processes for Reducing Wear and Corrosion, *Brit. Corros. J.*, 1999, **34**, p 171-183
2. F. Tang, L. Ajdelsztajn, G.E. Kim, V. Provenzano, and J.M. Schoenung, Effects of Surface Oxidation During HVOF Processing on the Primary Stage Oxidation of a CoNiCrAlY Coating, *Surf. Coat. Technol.*, 2004, **185**, p 228-233
3. P.K. Wright and A.G. Evans, Mechanisms Governing the Performance of Thermal Barrier Coatings, *Curr. Opin. Solid State Mat. Sci.*, 1999, **4**(3), p 255-265
4. A.G. Evans, D.R. Mumm, J.W. Hutchinson, G.H. Meier, and F.S. Pettit, Mechanisms Controlling the Durability of Thermal Barrier Coatings, *Prog. Mater. Sci.*, 2001, **46**(5), p 505-553
5. K. Messaoudi, A.M. Huntz, and B. Lesage, Diffusion and Growth Mechanism of Al_2O_3 Scales on Ferritic Fe-Cr-Al Alloys, *Mater. Sci. Eng. A*, 1998, **247**(1-2), p 248-262
6. C.J. Li and W.Y. Li, Effect of Sprayed Powder Particle Size on the Oxidation Behavior of MCrAlY Materials During High Velocity Oxygen-fuel Deposition, *Surf. Coat. Technol.*, 2002, **162**(1), p 31-41
7. H.B. Xiong, L.L. Zheng, L. Li, and A. Vaidya, Melting and Oxidation Behavior of In-flight Particles in Plasma Spray Process, *Int. J. Heat Mass Transf.*, 2005, **48**, p 5121-5133
8. C.J. Li and Y.Y. Wang, Effect of Particle State on the Adhesive Strength of HVOF Sprayed Metallic Coating, *J. Thermal Spray Technol.*, 2002, **11**(4), p 523-529
9. M.J. Pomeroy, Coatings for Gas Turbine Materials and Long Term Stability Issues, *Mater. Des.*, 2005, **26**, p 223-231
10. K. Shimotor and T. Aisaka, The Trend of MCrAlX Alloys for High-Temperature-Protective Coatings, *Tetsu To Hagane-J. Iron Steel Inst. Jpn.*, 1983, **69**(10), p 1229-1241, in Japanese
11. R. Anton, J. Birkner, N. Czech, and W. Stamm, Degradation of Advanced MCrAlY Coatings by Oxidation and Interdiffusion, *Mater. Sci. Forum*, 2001, **369-372**, p 719-726
12. K. Ogawa, K. Ito, T. Shoji, D.W. Seo, H. Tezuka, and H. Kato, Effects of Ce and Si Additions to CoNiCrAlY Bond Coat Materials on Oxidation Behavior and Crack Propagation of Thermal Barrier Coatings, *J. Thermal Spray Technol.*, 2006, **15**(4), p 640-651
13. J.A. Haynes, M.K. Ferber, W.D. Porter, and E.D. Rigney, Characterization of Alumina Scales Formed During Isothermal and Cyclic Oxidation of Plasma-Sprayed TBC Systems at 1150 °C, *Oxid. Met.*, 1999, **52**(1/2), p 31-76
14. J.R. Nicholls, N.J. Simms, W.Y. Chan, and H.E. Evans, Smart Overlay Coatings-Concept and Practice, *Surf. Coat. Technol.*, 2002, **149**, p 236-244
15. N. Czech, M. Juez-Lorenzo, V. Kolarik, and W. Stamm, Influence of the Surface Roughness on the Oxide Scale Formation on MCrAlY Coatings Studied In Situ by High Temperature X-ray Diffraction, *Surf. Coat. Tech.*, 1998, **108**(1-3), p 36-42
16. M.P. Taylor and H.E. Evans, The Influence of Bond Coat Surface Roughness and Structure on the Oxidation of a Thermal Barrier Coating System, *Mater. Sci. Forum*, 2001, **369**(3), p 711-717
17. U. Bardi, L. Carrafiello, R. Groppetti, F. Niccolai, G. Rizzi, A. Scrivani, and F. Tedeschi, On the Surface Preparation of Nickel Superalloys before CoNiCrAlY Deposition by Thermal Spray, *Surf. Coat. Tech.*, 2004, **184**(2-3), p 156-162
18. E. Lugscheider, C. Herbst, and L. Zhao, Parameter Studies on High-velocity Oxy-fuel Spraying of MCrAlY Coatings, *Surf. Coat. Technol.*, 1998, **108-109**, p 16-23
19. S. Sampath, X.Y. Jiang, J. Matejicek, L. Prchlik, A. Kulkarni, and A. Vaidya, Role of Thermal Spray Processing Method on the Microstructure, Residual Stress and Properties of Coatings: An Integrated Study for Ni-5 wt.%Al Bond Coats, *Mater. Sci. Eng. A*, 2004, **364**(1-2), p 216-231
20. A. Kulkarni, A. Vaidya, A. Goland, S. Sampath, and H. Herman, Processing Effects on Porosity-Property Correlations in Plasma Sprayed Yttria-Stabilized Zirconia Coatings, *Mater. Sci. Eng. A*, 2003, **359**(1/2), p 100-111
21. G. Espie, P. Fauchais, B. Hannoyer, J.C. Labbe, and A. Vardelle, Effect of Metal Particles Oxidation During the APS on the Wettability, *Ann.NY Acad.Sci.*, 1999, **891**, p 143-151
22. G. Espie, A. Denoirjean, P. Fauchais, J.C. Labbe, J. Dubsky, O. Schneeweiss, and K. Volenik, In-Flight Oxidation of Iron Particles Sprayed Using Gas and Water Stabilized Plasma Torch, *Surf. Coat. Technol.*, 2005, **195**, p 17-28
23. G. Espie, P. Fauchais, J.C. Labbe, A. Vardelle, and B. Hannoyer, Oxidation of Iron Particles During APS: Effect of the Process on Formed Oxide Wetting of Droplets on Ceramics Substrates, *Thermal Spray 2001: New Surfaces for a New Millennium*, C.C. Berndt, K.A. Khor, and E.F. Lugscheider, Ed., May 28-30, 2001 (Singapore), ASM International, 2001, p 821-827
24. O.P. Solonenko, M.A. Anatolyevich, K.E. Vladimirovich, B.M. Petrovna, K. Ogawa, T. Shoji, and M. Tanno, Theoretical Modeling and Experimental Study of Thermal Barrier Coatings, *Mater. Trans.*, 2003, **44**(11), p 2311-2321
25. K. Dobler, H. Kreye, and R. Schwetzke, Oxidation of Stainless Steel in the High Velocity Oxy-Fuel Process, *J. Therm. Spray Technol.*, 2000, **9**(3), p 407-413
26. T. Fukushima and S. Kuroda, Oxidation of HVOF Sprayed Alloy Coatings and Its Control by a Gas Shroud, *Thermal Spray 2001: New Surfaces for a New Millennium*, C.C. Berndt, K.A. Khor, and E.F. Lugscheider, Ed., May 28-30, 2001 (Singapore), ASM International, 2001, p 527-532
27. V. Gourlaouen, E. Verna, and P. Beaubien, Influence of Flame Parameters on Stainless Steel Coatings Properties, *Thermal Spray: Surface Engineering Via Applied Research*, C.C. Berndt, Ed., May 8-11, 2000 (Montréal, Québec, Canada), ASM International, 2000, p 487-493
28. V. Gourlaouen, E. Verna, K. Khor, and P.S.T. Guek, Role of Some Fuel Gases on Properties of HVOF Metallic Coatings, *Thermal Spray 2001: New Surfaces for a New Millennium*, C.C. Berndt, K.A. Khor, and E.F. Lugscheider, Ed., May 28-30, 2001 (Singapore), ASM International, 2001, p 519-525
29. R.A. Neiser, M.F. Smith, and R.C. Dykhuizen, Oxidation in Wire HVOF-Sprayed Steel, *J. Therm. Spray Technol.*, 1998, **7**(4), p 537-545
30. D. Seo, K. Ogawa, M. Tanno, T. Shoji, and S. Murata, Influence of Heat Exposure Time on Isothermal Degradation of Plasma Sprayed CoNiCrAlY Coatings, *Surf. Coat. Technol.*, 2007, **201**(18), p 7952-7960
31. J.A. Thompson and T.W. Clyne, The Effect of Heat Treatment on the Stiffness of Zirconia Top Coats in Plasma-Sprayed TBCs, *Acta Mater.*, 2001, **49**(9), p 1565-1575
32. H.H. Zhu, J.Y.H. Fuh, and L. Lu, The Influence of Powder Apparent Density on the Density in Direct Laser-Sintered Metallic Parts, *Int. J. Mach. Tool Manuf.*, 2007, **47**(2), p 294-298
33. V.K. Tolpygo and D.R. Clarke, Surface Rumpling of a (Ni, Pt)Al Bond Coat Induced by Cyclic Oxidation, *Acta Mater.*, 2000, **48**, p 3283-3293
34. H.M. Tawancy, N. Sridhar, N.M. Abbas, and D.S. Rickerby, Comparative Performance of Selective Bond Coats in Advanced Thermal Barrier Coating Systems, *J. Mater. Sci.*, 2000, **35**, p 3615-3629
35. H.S. Choi, B. Yoon, H.J. Kim, and C.H. Lee, Isothermal Oxidation of Air Plasma Spray NiCrAlY Bond Coatings, *Surf. Coat. Tech.*, 2002, **150**(2-3), p 297-308